# Investigation of carrier recombination at the $SiO_2$/c-Si interface by photoluminescence imaging under applied bias

Halvard Haug, Ørnulf Nordseth, Edouard Monakhov and Erik Stensrud Marstein

***Abstract*—A new technique for analyzing the surface recombination for passivated silicon substrates has been employed to study the $SiO_2$/c-Si interface under various band bending conditions. A photoluminescence imaging setup was used to measure the effective minority carrier lifetime of oxidized Si wafers while applying an external bias over the rear side passivation layer. This method was used to investigate both the effect of substrate doping polarity and post-oxidation forming gas anneal (FGA) upon the surface passivation properties. The measured carrier lifetimes as a function of voltage were interpreted in the framework of the extended Shockley-Read-Hall theory. The calculated oxide charge density was found to decrease from ~$7\times10^{11}$ $cm^{-2}$ to ~$4\times10^{11}$ $cm^{-2}$ after the FGA treatment for both p-type and n-type substrates, causing a reduction in the field effect passivation. On the contrary, an increased chemical passivation was observed after FGA, shown by a reduction of the effective surface recombination velocity parameters by a factor of 3.8-5.5. In total, a significant increase in the effective carrier lifetime was obtained for both substrate types. Furthermore, the carrier capture efficiency at the surface defects was found to be 2-2.5 times higher for electrons than for holes, regardless of doping polarity and FGA.**

***Index Terms*—Charge carrier lifetime, imaging, photoluminescence, silicon, surfaces**

## I. Introduction

In the development of high efficiency solar cells based on thin silicon wafers, reduction of electronic recombination at the wafer surfaces is a topic of high and increasing importance. The surface recombination velocity (SRV) at a silicon surface is proportional to the interface defect density and is limited by the availability of minority charge carriers near the surface. The recombination losses can therefore be reduced by lowering the interface defect density (chemical passivation) or by reducing the concentration of either electrons or holes in the region near the surface with a built-in electric field (field-effect passivation) [1]. Such band bending towards the surface is normally obtained in solar cells by applying a dielectric passivation layer incorporating fixed charges.

The SRV of a passivated Si surface is normally calculated from measurements of the effective minority charge carrier lifetime $\tau_{eff}$ (hereafter: lifetime), which contains contributions from recombination in the bulk of the wafer and at the two surfaces [2]. For characterization purposes, modulation of the surface band bending, and thus the SRV, is possible by applying voltage to a gate electrode placed on top of a dielectric passivation layer [3],[4],[5] or by deposition of charged ions on the surface in a corona discharge chamber [6],[7]. The latter method has traditionally been preferred in solar cell research, both because of its non-invasive nature and in order to avoid the necessity for making contacts to the sample. Additionally, the presence of metallic electrodes typically interferes with most of the common carrier lifetime measurements.

Recently we proposed a new technique for analyzing the surface recombination for passivated silicon substrates [8]. The technique is based on measurements of the effective lifetime in a photoluminescence (PL) imaging setup [9] while applying a voltage over the rear side passivation layer (PL-V). In contrast to corona charging techniques, PL imaging under applied bias requires the presence of metal electrodes on the sample surface. However, the method allows for very fast measurements and simultaneous data collection from multiple areas on the sample. The technique also has the advantage of allowing for repeated voltage sweeps between inversion and accumulation, which can be recorded with little or no influence of the measurement history of the sample.

Thermal oxidation is a well-established technology for surface passivation of Si substrates and can be implemented in both lab-scale and industrial solar cell processes [10]. The passivation properties of the c-Si/$SiO_2$ interface mainly arise from a high degree of chemical passivation, with a reported density of interface states $D_{it}$ as low as $10^9$ $cm^{-2}eV^{-1}$ [11]. Thermal $SiO_2$ layers may also give a moderate field-effect passivation, caused by positive fixed charges located at the interface, with a typical density in the range $1-5\times10^{11}$ $cm^{-3}$ [12]. In this paper we have used measurements of effective lifetime as a function of voltage (PL-V) to investigate the surface passivation properties of $SiO_2$ layers formed by high temperature dry oxidation. Furthermore, we present an interpretation of the surface passivation properties

This work has been funded by the Research Council of Norway through the project "Thin and highly efficient silicon-based solar cells incorporating nanostructures," NFR Project No. 181884/S1.

H. Haug, Ø. Nordseth and E. S. Marstein are with the Department of Solar Energy, Institute for Energy Technology, Kjeller 2027, Norway, (e-mail: halvard.haug@ife.no; ornulf.nordseth@ife.no; erik.stensrud.marstein@ife.no).

H. Haug, E. Monakhov and E. S. Marstein are with the Department of Physics, University of Oslo, Blindern, Oslo 0316, Norway

in terms of the oxide charge density and the effective surface recombination parameters for electrons and holes.

## II. Experimental Details

Samples were made from double side polished and thermally oxidized FZ Si (100) wafers. Both n-type (P-doped) and p-type (B-doped) substrates were used, with doping concentrations of $1.7\times10^{15}$ and $5.0\times10^{15}$ $cm^{-3}$, and thicknesses of 290 and 280 µm, respectively. The wafers had a high bulk lifetime to ensure that the measured effective lifetime was dominated by recombination at the wafer surfaces.

After a standard RCA (1+2) clean and 30 s immersion in a 5% HF solution, the wafers were loaded into a tube furnace and oxidized in dry $O_2$ at 1000 °C for 60 min. The resulting thermal $SiO_2$ layers provide a stable, high quality surface passivation with negligible leakage current, simplifying the interpretation of the results. Subsequently, one wafer of each doping polarity received a post-oxidation forming gas anneal (FGA) with 5% $H_2$ in $N_2$ at 400 °C for 30 min. This process is commonly used in the literature to reduce the number of interface states by hydrogen diffusion and passivation of dangling bonds [1]. The oxide thickness was measured by variable-angle spectroscopic ellipsometry and found to be 66-68 nm uniformly across the wafers.

7 mm × 7 mm square electrodes for PL-V measurements and 0.45-2.25 mm diameter circular electrodes for capacitance vs. voltage (C-V) measurements were deposited onto the oxide layers by thermal evaporation of Al through a shadow mask. Finally, low resistivity contacts were made to the Si substrate by grinding down the oxide with P200 sand paper and depositing Ag by thermal evaporation in the region opposite the C-V electrodes.

A schematic overview of the experimental setup for the PL-V method is shown in Fig. 1. Steady state carrier lifetime measurements were carried out with a LIS-R1 PL imaging setup from BT imaging with an excitation wavelength of 808 nm and a constant illumination intensity of 33.4 mW/cm$^2$. In a PL imaging lifetime measurement, the excess minority carrier concentration (injection level) at each point of the image is calculated from the measured PL intensity. For a p-type sample $\Delta n$ is given by

$$\Delta n = \sqrt{\left(\frac{N_A}{2}\right)^2 + \frac{I_{PL}}{C_{cal}}} - \frac{N_A}{2}, \qquad (1)$$

where $N_A$ is the acceptor doping concentration, $I_{PL}$ is the measured PL intensity and $C_{cal}$ is an instrument- and sample specific calibration constant, which is determined from a quasi-steady state photoconductance (QSSPC) measurement [13]. For the PL-V measurements, a reference region without metal electrodes was used for this purpose. An external voltage source was connected to the sample as shown in Fig. 1 in order to perform the measurements with an applied bias over the rear side passivating oxide layer. The PL intensity in the region over the Al electrodes is enhanced compared to the reference region due to an increased rear side reflectance, ausing a larger fraction of the emitted PL light to reach the camera. To account for this, $I_{PL}$ in the region above the metal electrodes was divided by an optical enhancement factor of 1.36. This factor is sample specific and was determined experimentally by measuring the enhancement of the PL intensity after placing the sample over an Al mirror made by thermal evaporation of 100 nm Al on a glass substrate. The steady state effective lifetime image was then calculated from the measured injection level averaged over the electrode area as $\tau_{eff} = \Delta n/G$ , where $G$ is the excess carrier generation rate per volume. An extensive discussion of the optical corrections and other possible errors in the calculation of $\tau_{eff}$ is described elsewhere [14]. A typical PL lifetime image measured while applying voltage over the rear side passivation layer is shown in Fig. 2.

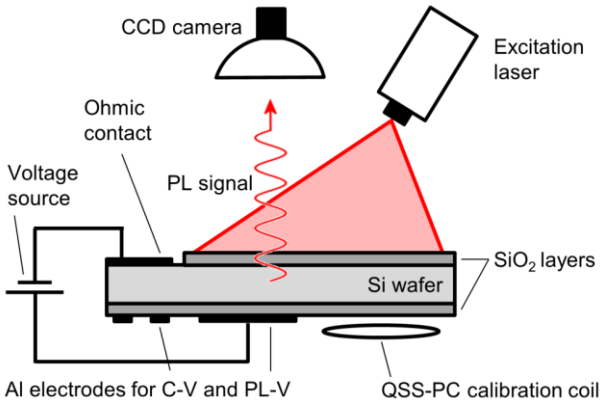


Fig. 1. Schematic overview of the experimental setup for the PL-V method, used to obtain lifetime images while modulating the surface band bending by applying voltage over the rear side passivation layer. Al electrodes for both C-V and PL-V measurements are present on each sample.

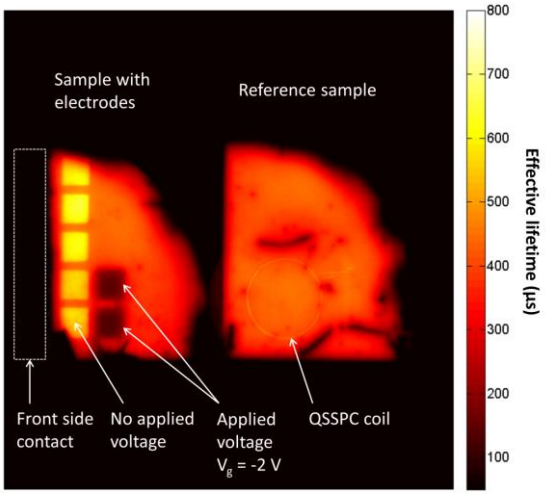


Fig. 2. PL lifetime image measured on the p-type wafer after FGA treatment while applying a voltage of -2 V over two of the rear Al electrodes. In this case a quarter of the wafer (right) is used for lifetime calibration, whereas Al electrodes are deposited on another quarter (left). Note that the PL signal is larger above the Al electrodes not under bias compared to the surrounding areas, due to the built-in voltage from the Al-Si work function difference and an increased rear reflectance. The C-V electrodes are hidden behind the front side contact covering the left hand side of the left quarter (see Fig. 1).

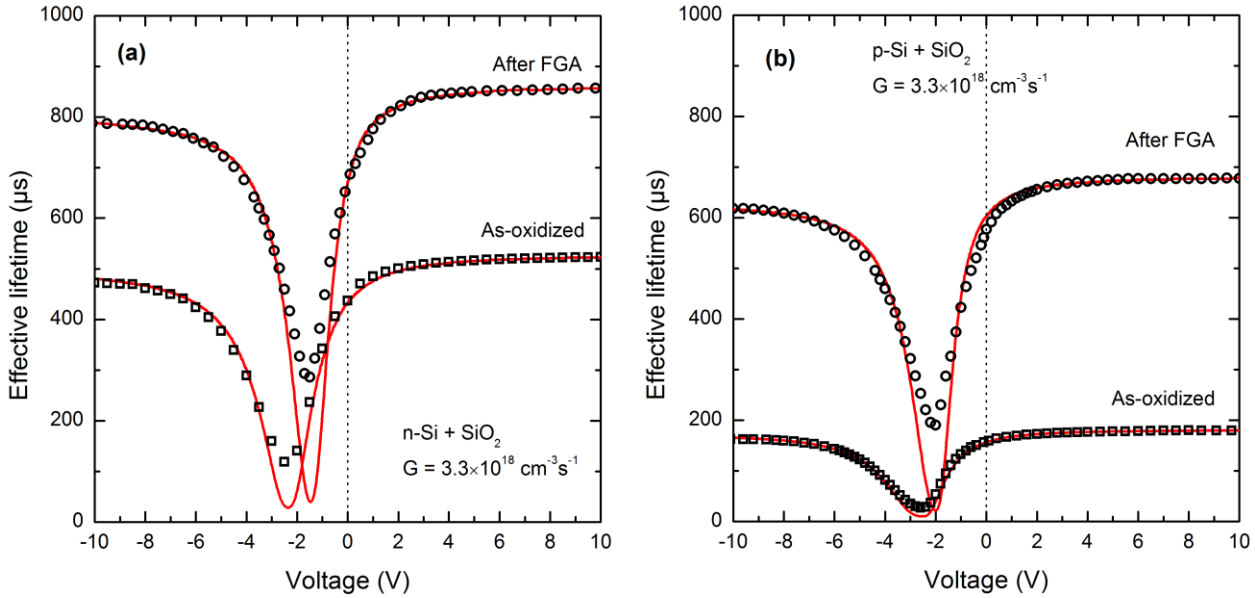


Fig. 3. Effective lifetime of the n-type (a) and the p-type (b) samples as a function of voltage applied to one of the sample surfaces, before and after FGA. The measurements were performed using a constant generation rate of G = $3.3\times10^{18}$ $cm^{-3}s^{-1}$. The experimental data is shown as open symbols, whereas the simulated curves are shown as solid red lines. The simulation details are given in section IV-B and the simulation parameters are given in Table I. The line corresponding to zero applied voltage is indicated by a dotted vertical line for clarity.

The fixed oxide charge density $Q_{ox}$ in the $SiO_2$ layers was extracted from high frequency (1 MHz) C-V curves measured using a Keithley 4200-SCS semiconductor characterization system. The fixed charge density per $cm^2$ is calculated as

$$Q_{ox} = C_{ox}(\phi_{ms} - V_{fb})/q, \qquad (2)$$

where $C_{ox}$ is the measured oxide capacitance per unit area, $q$ is the elementary charge, $\phi_{ms}$ is the metal-semiconductor work function and $V_{fb}$ is the flat band voltage. $V_{fb}$ is the voltage that is needed to obtain zero band bending at the Si surface, and can be extracted from the C-V curve following the procedure described in [15]. For a p-type sample $\phi_{ms}$ is calculated as

$$\phi_{ms} = F_m - \chi_{Si} - \frac{E_g}{2} - \frac{k_B T}{q}\ln\left(\frac{N_A}{n_i}\right), \qquad (3)$$

where $F_m$ is the metal work function, $\chi_{Si}$ is the electron affinity of Si, $E_g$ is the band gap, $k_B$ is the Boltzmann constant, $T$ is the temperature and $n_i$ is the intrinsic carrier concentration. Using an Al work function of 4.1 eV and $\chi_{Si} = 4.05$ eV, $\phi_{ms}$ was calculated to be -0.84 eV for the p-type samples and $-0.2$ eV for the n-type samples. Results from between 10 and 15 measurements using different electrode sizes were averaged in the calculation of $Q_{ox}$.

## III. Results

### A. *Effective lifetime vs. voltage*

Fig. 3 shows the effective carrier lifetime of the n-type and p-type samples as a function of the applied gate voltage $V_g$. For both types of substrate doping the effective lifetime increases after FGA. All the carrier lifetime vs. voltage curves show the same general behavior: When a small negative voltage is applied the effective lifetime decreases as the external bias compensates the effect of the positive oxide charge density. For increasing negative voltages, the lifetime drops to a minimum corresponding to depletion conditions at the surface, before it increases as the surface is driven into inversion (n-type samples) or accumulation (p-type samples). The curves are slightly asymmetric, with a lower effective lifetime for large negative voltage as compared to large positive voltage.

The minimum lifetime in the PL-V curve in the as-oxidized state and after FGA is found to be 119 µs and 286 µs for the n-type sample and 27 µs and 190 µs for the p-type sample, respectively. The highest lifetime was observed in the n-type sample under accumulation conditions; with $\tau_{eff} = 856$ µs. Note that all lifetime images were measured using a constant generation rate, so that the injection level $\Delta n$ changes with the lifetime in the sample according to the relation $\Delta n = \tau_{eff} G$. For instance, in the n-type sample after FGA the lifetime variation corresponds to injection levels in the range between $9.4 \times 10^{14}$ $cm^{-3}$ and $2.8 \times 10^{15}$ $cm^{-3}$.

### B. *Capacitance-voltage measurements*

Typical C-V curves measured on the p-type sample are shown in Fig. 4. The flat band voltage was observed to decrease after forming gas anneal, indicating a lowering of the oxide charge density. Average $Q_{ox}$ values, calculated from 10-15 measurements on each sample, are presented in Table I.

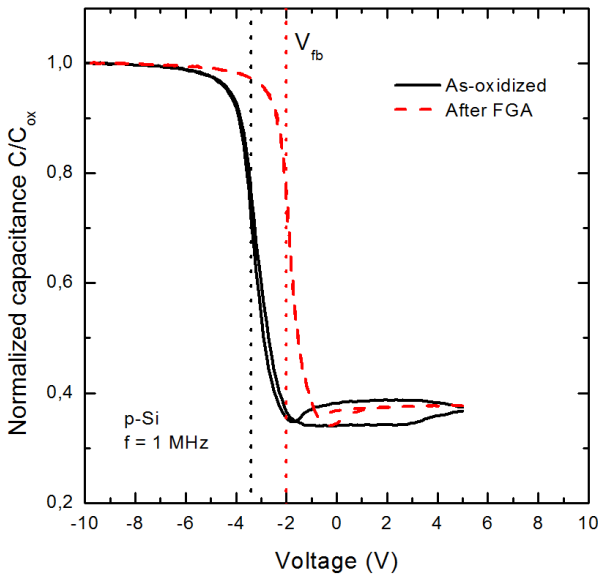


Fig. 4. Normalized C-V curves measured on the p-type sample, before (solid line) and after (dashed line) FGA treatment. The flat band voltage $V_{fb}$ (indicated by dotted lines) is reduced after FGA treatment.

## IV. Analysis and Discussion

### A. Calculation of experimental SRV values

In order to obtain a more fundamental understanding of the data presented in Fig. 3, front and rear SRVs were calculated from the lifetime measurements in the following manner: The front side SRV $S_f$ was first calculated from the effective lifetime $\tau_{eff}$ measured by QSSPC in the reference region, where the front and rear SRVs are assumed to be identical [2]:

$$S_f = \alpha D \tan\left(\frac{\alpha W}{2}\right). \quad (4)$$

Here $D$ is the minority carrier diffusion coefficient, $W$ is the wafer thickness and $\alpha$ is given by

$$\alpha = \sqrt{\frac{1}{D}\left(\frac{1}{\tau_{eff}} - \frac{1}{\tau_{bulk}}\right)}, \quad (5)$$

where $\tau_{bulk}$ is the bulk lifetime. It should be noted that the effective lifetime in the reference region does not directly correspond to the lifetime measured at 0 V in the PL-V curves, as the lifetime over the electrodes is also influenced by the change in rear SRV caused by the built-in potential due to $\phi_{ms}$. The rear side SRV $S_r$ was then calculated from $S_f$ and the measured lifetime, over the active electrode at each point of the curves shown in Fig. 3 as [2]:

$$S_r = \frac{\tan(\alpha W)\,\alpha^2 D^2 - \alpha D S_f}{\alpha D + \tan(\alpha W)\,S_f}, \quad (6)$$

with $\alpha$ defined as above. FZ wafers with a high bulk lifetime were used in the experimental investigation to ensure that the contribution from bulk recombination is small. Still, the chosen value for $\tau_{bulk}$ has some influence on the result. To ensure that the bulk lifetime did not significantly degrade after oxidation a quarter of each wafer was dipped in a 5% HF solution for 1 min to strip off the oxide layers, cleaned by a standard RCA 1+2 clean, dipped in 5% HF solution for 30 s and passivated on both sides with a 40 nm thick layer of hydrogenated amorphous Si (a-Si:H) deposited by plasma enhanced chemical vapor deposition. This surface passivation layer ensures a SRV less than 5 cm/s, and thus the measured effective lifetime of these samples give a good indication of the bulk lifetime. Based on these measurements a constant bulk lifetime of 5 ms was chosen for the calculations, and the error bars on the SRV values were calculated using $\tau_{bulk} = 2.5$ ms and $\tau_{bulk} = \infty$ ms as minimum and maximum values. The calculated values for $S_f$ and $S_r$ as a function of $V_g$ for the p-type sample after FGA treatment is shown in Fig. 5.

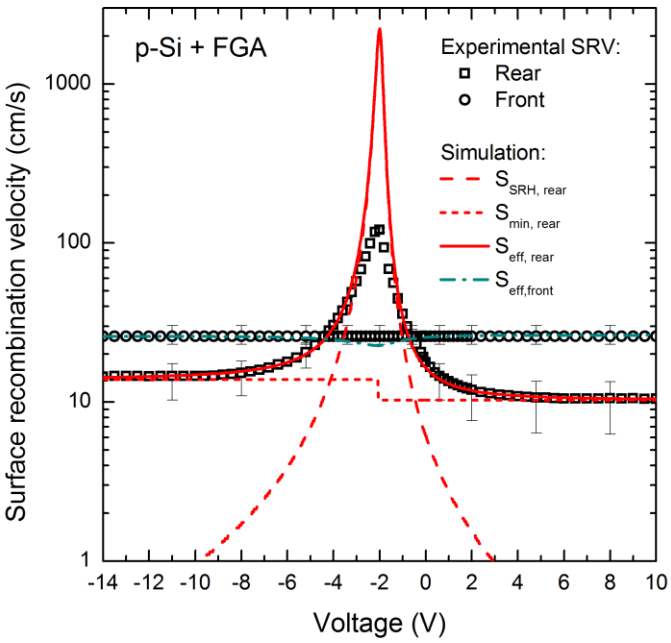


Fig. 5. Front and rear side SRV for the p-type sample after FGA as a function of applied voltage. Experimental values (calculated from the measured carrier lifetime data shown in Fig. 3) are plotted together with the different simulated contributions to the effective SRV. Error bars are calculated from minimum and maximum bulk lifetime values.

### B. Simulation of the effective SRV

Measurements of effective lifetime (and thus the SRV) with varying surface potential allow for a fundamental understanding of the surface recombination mechanisms, and are particularly useful for separating the contributions from field-effect and chemical passivation. In order to quantitatively extract fundamental properties of the interface traps responsible for carrier recombination we have fitted the results to an extended Shockley-Read Hall (SRH) recombination model [16]. No measurements of the (energy dependent) interface state density $D_{it}$ or capture cross sections $\sigma_{n/p}$ have been performed for this work. A simplified model including one effective midgap defect level was therefore

chosen, and was found to sufficiently describe the observations. The rear effective SRV is then given from standard SRH theory as

$$S_{SRH} = \frac{1}{\Delta n} \frac{S_{n0} S_{p0} (n_s p_s - n_i^2)}{S_{n0}(n_s + n_i) + S_{p0}(p_s + n_i)}, \quad (7)$$

where $n_i$ is the intrinsic carrier concentration and $S_{n0}$ and $S_{p0}$ are the SRV parameters of electrons and holes, defined as the product of the electron thermal velocity $v_{th}$, the concentration of surface states per unit area $N_{it}$ and the corresponding capture cross section $\sigma_n$ or $\sigma_p$. The surface concentrations of electrons and holes $n_s$ and $p_s$ are strongly dependent on the surface potential $\psi_s$. We use the so-called Girisch formalism [3], [16] to numerically find a self-consistent value for $\psi_s$ (and thus $n_s$ and $p_s$) for any given values for $V_g$, $Q_{ox}$ and $\phi_{ms}$. This method is based upon a numerical solution of the charge balance at the interface, under the assumption of constant quasi Fermi levels throughout the surface space charge region. To simplify the analysis we have assumed that $Q_{ox}$ is constant with all the charges located at the c-Si/$SiO_2$ interface and that the contribution from the charges in the interface traps $Q_{it}$ can be neglected in the charge balance.

As seen on the experimental SRVs shown in Fig. 5, the SRV could not be enforced arbitrarily low by increasing the voltage, but instead it reaches a minimum value. It was therefore necessary to add a (voltage-independent) contribution to the effective SRV called $S_{min}$ in order to correctly describe the flattening of the lifetime vs. voltage curves under large surface band bending:

$$S_{eff} = S_{SRH} + S_{min}. \quad (8)$$

Note that this effect could not be accounted for by recombination at the front surface or in the bulk of the wafers. A similar approach has also previously been used for such simulations [7],[12]. In these works inclusion of shunt and recombination currents through the space-charge region were used to theoretically describe measurements of the SRV as function of surface charge and injection level.

The measured minimum SRV was found to be different for large negative voltages compared to large positive voltages. $S_{min}$ was therefore modeled as

$$S_{min} = \begin{cases} S_{min,n} \text{ for } \psi_s < 0 \\ S_{min,p} \text{ for } \psi_s > 0. \end{cases} \quad (9)$$

### C. Simulation results

The model described above was used to numerically calculate the effective SRV for each value of $V_g$. A least squares optimization algorithm was then used find a best fit between the model and the front and rear experimental SRVs, with $S_{0n}$, $S_{0p}$, $Q_{ox}$, $S_{min,n}$ and $S_{min,p}$ used as free fitting parameters. When simultaneously fitting the model to both $S_r$ and $S_f$ it is possible to find a relatively unique fit, as each parameter plays a different role in the determination of the curve: $S_{n0}$ and $S_{p0}$ determine the slope of the left and right hand side of the SRV peak, $Q_{ox}$ determines the position of the lifetime minimum along the voltage axis, and $S_{min,n}$ and $S_{min,p}$ determine the minimum SRV at large negative and large positive voltages, respectively. The simulated effective lifetime for each measurement is shown in Fig. 3 and the different SRV contributions are shown in Fig. 5 for the p-type sample after FGA. The best fit parameters for each measurement are given in Table I, together with the average $Q_{ox}$ values calculated from C-V measurements.

From Table I it can be seen that both $S_{n0}$ and $S_{p0}$ are reduced after FGA for both substrate polarities. The ratio between the capture cross sections for electrons and holes $\sigma_n / \sigma_p$ (given by $S_{n0}/S_{p0}$) are however found to approximately constant, and is found to be between 2 and 2.5 for all measurements, regardless of doping polarity and FGA treatment. Knowledge of this ratio is valuable as it can aid in an identification of the type of defect which is dominating the recombination. It is also interesting from a technological point of view, as the ratio between $\sigma_n$ and $\sigma_p$ affects the injection level dependence of the SRV, which again is a contributing factor to the fill factor of high-efficiency Si solar cells with passivated rear surfaces.

The minimum SRV values $S_{min,n}$ and $S_{min,p}$ are also observed to decrease after FGA, with $S_{min,n}$ being larger than $S_{min,p}$ for all the curves. This is consistent with $\sigma_n$ being larger than $\sigma_p$ at the interface defects.

Furthermore, $Q_{ox}$ is found to decrease from $6-7\times10^{11}$ to $\sim4\times10^{11}$ $cm^{-3}$ after FGA for both samples, caused by a shift of the lifetime minimum towards lower negative voltages in the PL-V curves. This is in good agreement with the results from the C-V measurements, shown in the lower part of Table I. The observed reduction of both the oxide charge and the effective SRV parameters (and thus $D_{it}$) is consistent with previous findings in the literature [1, p. 118].

### D. Possible errors and deviations

Using the best-fit parameters the model described in section IV-B gives a good simultaneous agreement with the measured front and rear SRVs under most band bending conditions. The SRH model however overestimates the rear SRV in the region of the curve corresponding to depletion conditions (close to $V_{fb}$) by more than one order of magnitude. In this region the applied voltage counteracts the field-effect passivation from the oxide charges, and the rear SRV goes through a maximum where it is limited by chemical passivation only. This discrepancy suggests that the model described in section IV-B cannot fully describe the surface recombination behavior when the SRV is large. A possible explanation for this may be that the assumption of constant quasi-Fermi levels throughout the surface space region which is used in [3] may not hold for the largest SRVs observed at depletion conditions.

The error bars indicated in Fig. 5 are calculated based on an uncertainty in the bulk lifetime of the samples. This possible

TABLE I
SIMULATION PARAMETERS AND $Q_{OX}$ VALUES CALCULATED FROM THE C-V MEASUREMENTS.

| | Parameter | Description | Unit | n-type sample | | p-type sample | |
|---|---|---|---|---|---|---|---|
| | | | | As-oxidized | FGA | As-oxidized | FGA |
| **Fitting parameters for simulations** | $S_{n0}$ | SRV parameter for electrons | cm/s | 12000 | 3300 | 21000 | 2500 |
| | $S_{p0}$ | SRV parameter for holes | cm/s | 5700 | 1300 | 8800 | 990 |
| | $S_{min,\,n}$ | Minimum SRV, $\psi_s < 0$ | cm/s | 21 | 9.1 | 61 | 14 |
| | $S_{min,\,p}$ | Minimum SRV, $\psi_s > 0$ | cm/s | 17 | 6.6 | 53 | 10 |
| | $Q_{ox}$ | Fixed oxide charge | $cm^{-2}$ | $6.8\times10^{11}$ | $3.7\times10^{11}$ | $6.1\times10^{11}$ | $4.0\times10^{11}$ |
| **C-V analysis** | $Q_{ox}$ | Fixed oxide charge | $cm^{-2}$ | $7.3\times10^{11}$ | $2.7\times10^{11}$ | $6.9\times10^{11}$ | $3.5\times10^{11}$ |
| | | Standard deviation | $cm^{-2}$ | $0.3\times10^{11}$ | $0.5\times10^{11}$ | $0.4\times10^{11}$ | $0.2\times10^{11}$ |

error is however the same for all points along the curve, so the conclusions based on relative differences, e.g. the difference between $S_{min,n}$ and $S_{min,p}$, are still valid. No significant charge build-up was observed during the course of the measurement, meaning that the points along the voltage-lifetime curve could be almost perfectly reproduced when the measurements were repeated without moving the sample. This is consistent with a very small hysteresis in the C-V curves shown in Fig. 3, which implies that $Q_{ox}$ is not changed during the measurement.

## V. CONCLUDING REMARKS

The PL-V technique has been shown to give reproducible results which are in agreement with both capacitance-voltage measurements and previous findings in the literature. Analysis of the PL-V curves using an extended SRH model gives valuable information about the passivation mechanisms, and can be used to separate the contributions from field-effect and chemical passivation. The method may be used to determine $S_{n0}$, $S_{p0}$ and $Q_f$ for a wide range of dielectric passivation layers, and in combination with supplementary measurements of the interface state density $D_{it}$ the method can also be used to determine the absolute values of $\sigma_n$ and $\sigma_p$ for the recombination active defects at the interface. The PL-V method allows for very fast measurements to be carried out independently of the measurement history of the sample, and gives the possibility of simultaneous measurements of several areas of the wafer. PL-V measurements can therefore be used as an attractive alternative method for characterization of Si surface passivation layers.

## ACKNOWLEDGMENT

The authors wish to thank Tine Uberg Nærland for valuable input and discussion of the manuscript and Marie Syre Wiig for help with the thermal oxidation process and forming gas annealing of the wafers.

## REFERENCES

[1] A. G. Aberle, "Crystalline silicon solar cells - Advanced surface passivation and analysis". Centre for Photovoltaic engineering, University of New South Wales, 1999.

[2] A. B. Sproul, "Dimensionless solution of the equation describing the effect of surface recombination on carrier decay in semiconductors," *J. Appl. Phys*, vol. 76, no. 5, pp. 2851–2854, 1994.

[3] R. B. M. Girisch, R. P. Mertens, and R. F. De Keersmaecker, "Determination of Si-$SiO_2$ interface recombination parameters using a gate-controlled point-junction diode under illumination," *IEEE Trans. Electron. Devices*, vol. 35, no. 2, pp. 203–222, 1988.

[4] E. Yablonovitch, R. M. Swanson, W. D. Eades, and B. R. Weinberger, "Electron-hole recombination at the Si-$SiO_2$ interface," *Appl. Phys. Lett.*, vol. 48, no. 3, pp. 245–247, 1986.

[5] W. E. Jellett and K. J. Weber, "Accurate measurement of extremely low surface recombination velocities on charged, oxidized silicon surfaces using a simple metal-oxide-semiconductor structure," *Appl. Phys. Lett.*, vol. 90, no. 4, pp. 042104–042104-3, 2007.

[6] M. Schofthaler, R. Brendel, G. Langguth, and J. H. Werner, "High-quality surface passivation by corona-charged oxides for semiconductor surface characterization," in *Proc. 1st World Conf. Photovoltaic Energy Convers.*,Waikoloa, HI 1994, vol. 2, pp. 1509-1512.

[7] S. W. Glunz, D. Biro, S. Rein, and W. Warta, "Field-effect passivation of the $SiO_2$ Si interface," *J. Appl. Phys*, vol. 86, no. 1, pp. 683-691, 1999.

[8] H. Haug, Ø. Nordseth, E. V. Monakhov, and E. S. Marstein, "Photoluminescence imaging under applied bias for characterization of Si surface passivation layers," *Sol. Energy Mater. Sol. Cells*, vol. 106, pp. 60–65, 2012.

[9] T. Trupke, R. A. Bardos, M. C. Schubert, and W. Warta, "Photoluminescence imaging of silicon wafers," *Appl. Phys. Lett.*, vol. 89, no. 4, pp. 44103–44107, 2006.

[10] D. Biro, S. Mack, A. Wolf, A. Lemke, U. Belledin, D. Erath, B. Holzinger, E. A. Wotke, M. Hofmann, L. Gautero, S. Nold, J. Rentsch, and R. Preu, "Thermal oxidation as a key technology for high efficiency screen printed industrial silicon solar cells," *Proc. 34th IEEE Photovoltaic Spec. Conf.*, Philadelphia, PA, 2009. pp. 1594–1599.

[11] A. G. Aberle, S. W. Glunz, A. W. Stephens, and M. A. Green, "High-eficiency silicon solar cells: $Si/SiO_2$ interface parameters and their impact on device performance," *Prog. Photovoltaic Res. Appl,*, vol. 2, no. 4, pp. 265–273, 1994.

[12] S. Mack, A. Wolf, C. Brosinsky, S. Schmeisser, A. Kimmerle, P. Saint-Cast, M. Hofmann, and D. Biro, "Silicon Surface Passivation by Thin Thermal Oxide/PECVD Layer Stack Systems,"*IEEE J. Photovoltaics*, vol. 1, no. 2. pp. 135–145, 2011.

[13] R. A. Sinton, A. Cuevas, and M. Stuckings, "Quasi-Steady-State PhotoConductance, A new method for solar cell material and device characterization," in *Proc. 25th IEEE Photovoltaic Spec. Conf.*, Washington, DC, 1996, pp. 457-460.

[14] H. Haug, S. Olibet, Ø. Nordseth, and E. S. Marstein, "Modulating the field-effect passivation at the $SiO_2$/c-Si interface: Analysis and verification of the photoluminescence imaging under applied bias method," *J. Appl. Phys,* to be published.

[15] D. K. Schroeder, "Semiconductor material and device characterization", 3rd ed. John Wiley & Sons, Inc., Hoboken, New Jersey., 2006, p. 334.

[16] A. G. Aberle, S. Glunz, and W. Warta, "Impact of illumination level and oxide parameters on Shockley--Read--Hall recombination at the $Si-SiO_2$ interface," *J. Appl. Phys*, vol. 71, no. 9, pp. 4422–4431, 1992.